ELSEVIER

Contents lists available at ScienceDirect

Archives of Biochemistry and Biophysics

journal homepage: www.elsevier.com/locate/yabbi



Effect of solvent viscosity on the activation barrier of hydrogen tunneling in the lipoxygenase reaction

Luis Guevara ^a, Melissa Gouge ^b, Amanda Ohler ^a, S. Gage Hill ^a, Soham Patel ^a, Adam R. Offenbacher ^a, ^{*}

ARTICLE INFO

Keywords: Hydrogen tunneling Solvent slaving Protein dynamics Lipoxygenase Enzyme kinetics

ABSTRACT

Hydrogen tunneling in enzyme reactions has played an important role in linking protein thermal motions to the chemical steps of catalysis. Lipoxygenases (LOXs) have served as model systems for such reactions, showcasing deep hydrogen tunneling mechanisms associated with enzymatic C–H bond cleavage from polyunsaturated fatty acids. Here, we examined the effect of solvent viscosity on the protein thermal motions associated with LOX catalysis using trehalose and glucose as viscogens. Kinetic analysis of the reaction of the paradigm plant orthologue, soybean lipoxygenase (SLO), with linoleic acid revealed no effect on the first-order rate constants, k_{cat} , or activation energy, E_{a} . Further studies of SLO active site mutants displaying varying E_{a} s, which have been used to probe catalytically relevant motions, likewise provided no evidence for viscogen-dependent motions. Kinetic analyses were extended to a representative fungal LOX from M. oryzae, MoLOX, and a human LOX, 15-LOX-2. While MoLOX behaved similarly to SLO, we show that viscogens inhibit 15-LOX-2 activity. The latter implicates viscogen sensitive, conformational motions in animal LOX reactions. The data provide insight into the role of water hydration layers in facilitating hydrogen (quantum) tunneling in LOX.

1. Introduction

Enzymes are inherently dynamic macromolecules. The role of protein thermal motions in bond cleavage steps is particularly evident in the case of non-classical, hydrogen tunneling enzyme reactions [1–3]. In emerging analytical models used to quantify these proton-coupled electron transfer (PCET) reactions [4], the coordinate that describes hydrogen wave function overlap is inherently temperature independent. Thus, the increase of the enzyme rate constant with temperature (i.e., $E_a(H) > 0$ kcal/mol) for rate-limiting and irreversible hydrogen tunneling arises from the need for environmental reorganization and thermal sampling of the protein conformations, with only a subset of productive conformers capable of achieving the proper reduction in donor-acceptor distances (DADs) and active site geometries that are effective for hydrogen wave function overlap [5]. Given the source of thermal energy that controls the structure and flexibility of proteins originates from the solvent [6–8], identifying the role that solvent plays

in influencing catalysis is an important step towards increasing the success of *de novo* biocatalyst design.

The lipoxygenase (LOX) family of enzymes has provided one of the most compelling systems for hydrogen tunneling in biology. LOXs are a family of mononuclear, non-heme metalloenzymes that oxidize polyunsaturated fatty acids to form potent, bioactive cell signaling mediators [9–11]. The initial and often rate limiting step in the lipoxygenase reaction is the homolytic C–H bond cleavage at a bis-allylic carbon of the fatty acid (Scheme 1). The formal hydrogen atom (H•) is transferred through a deep tunneling mechanism [12]. Soybean lipoxygenase (SLO) is the most well characterized system. The oxidation reaction of substrate linoleic acid by SLO (Scheme 1) exhibits an inflated primary deuterium kinetic isotope effect on the first order rate constant, ${}^{D}k_{\text{cat}}$, of ~60 that is weakly temperature dependent ($\Delta E_a = E_a(D) - E_a(H) = 0.9$ kcal/mol) [13]. The observation of ΔE_a ~0 kcal/mol is a clear kinetic marker for non-classical, quantum tunneling in biological catalysis [12].

Recently, a defined, anisotropic protein network, initiating at a

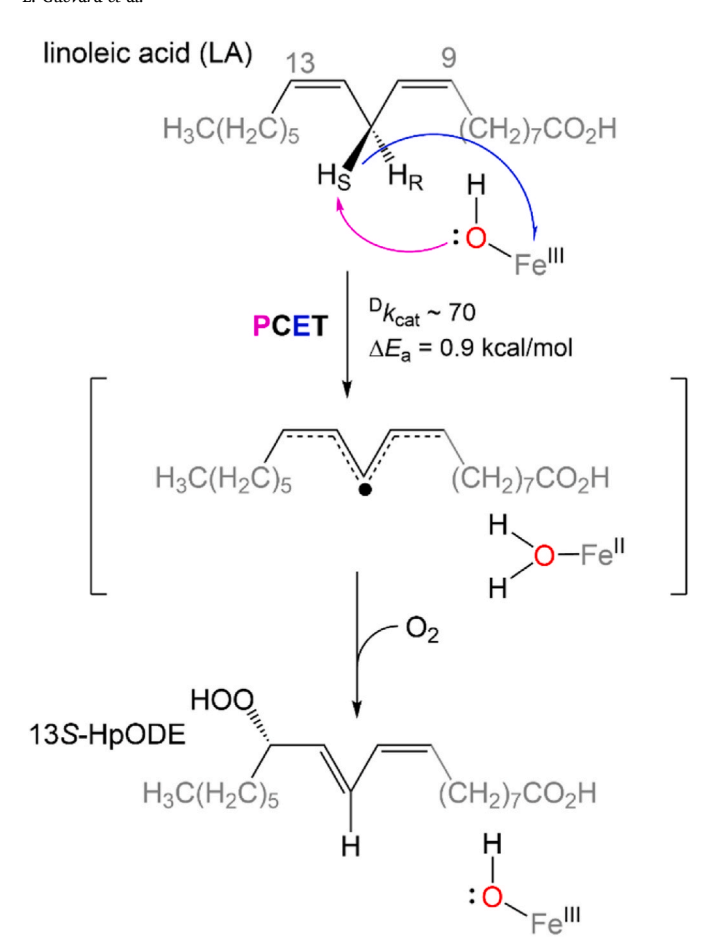
Abbreviations: LOX, lipoxygenase; SLO, soybean lipoxygenase; E_a , activation energy; 15-LOX2, human epithelial 15-lipoxygenase-2; MoLOX, M. oryzae lipoxygenase; DSC, differential scanning calorimetry; PCET, proton-coupled electron transfer; DAD, donor-acceptor distance; HDX-MS, hydrogen-deuterium exchange mass spectrometry; LA, linoleic acid; AA, arachidonic acid; PLAT, polycystin-1-lipoxygenase α -toxin; PTM, post-translational modification.

E-mail address: offenbachera17@ecu.edu (A.R. Offenbacher).

^a Department of Chemistry, East Carolina University, Greenville, NC, 27858, USA

^b Department of Chemistry and Biochemistry, Ohio Northern University, Ada, OH, 45810, USA

^{*} Corresponding author.



Scheme 1. Reaction mechanism for the oxidation of substrate linoleic acid, LA, by SLO. C–H cleavage occurs by a proton transfer (purple) coupled to electron transfer (blue), or PCET, process. Relevant kinetic isotope effects characteristic of hydrogen tunneling are listed. The rate-determining step is associated with C–H cleavage.

solvent-exposed loop, has been identified in SLO (Fig. 1A) and proposed to facilitate the tunneling process at the active site [14,15]. How the solvent interacts with this loop to mediate thermal energy transfer in SLO is not yet well known. In addition to temperature, the viscosity of solvent may also influence protein structural changes and dynamics. For example, altered dynamics of the bulk solvent from increased viscosity can affect slow, large scale protein structural rearrangements [6,16]. These viscosity-dependent protein motions are also referred to as 'solvent-slaved' [17]. If slaved protein motions are linked to tunneling effects at the active site, increased solvent viscosity will have deleterious effects on the catalytic rate constants [18,19]. Thus, modulating the solvent viscosity can help to shed light onto the role of solvent dynamics on tunneling efficiency.

Herein, we present a kinetic investigation on the impact of solvent viscosity on the activation barrier(s) for hydrogen tunneling in lipoxygenases. Both trehalose, a disaccharide, and glucose, a monosaccharide, were used to control the solvent viscosity. Our findings reveal that the protein motions necessary for enhancing tunneling probabilities in SLO are likely coupled to the hydration shell. In addition, two SLO variants with active site mutations that are associated with altered activation barriers for C–H cleavage and influence the nature of the protein dynamics were also examined. Viscosity effects were also expanded to the reactions of two other distinct LOXs, with a representative from each of the animal and fungi kingdoms. The cumulative results provide insight into the nature of the protein motions that facilitate and enhance the probability of hydrogen (quantum) tunneling occurring under biologically relevant conditions.

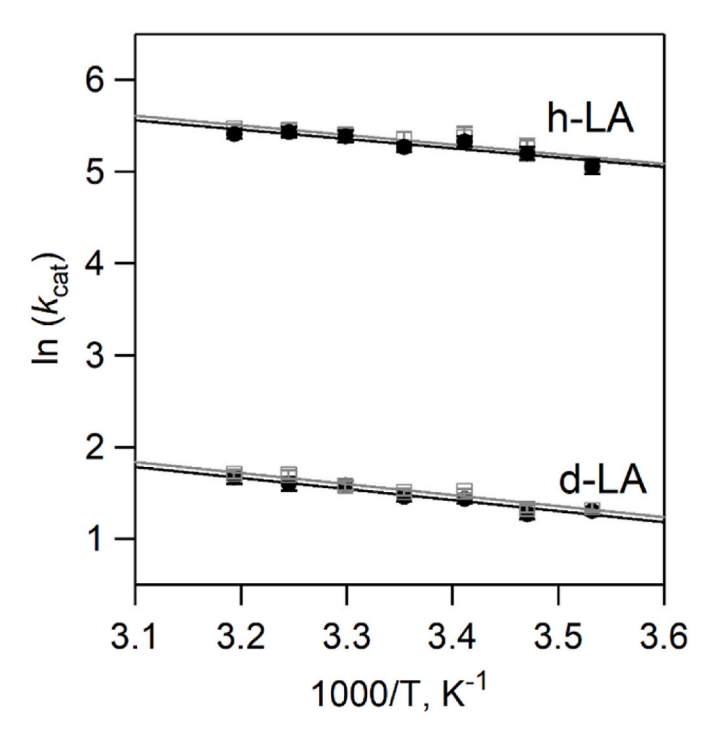


Fig. 1. Arrhenius plot of SLO reaction with h_{31} -LA and d_{31} -LA in the absence (black) and presence (gray) of 30% trehalose.

2. Experimental

Materials. AA and LA were purchased from Cayman Chemical Company (Ann Arbor, MI). D_{31} -linoleic acid methyl ester (98% D) was acquired from Cambridge Isotopes (Tewksbury, MA) and was converted to LA by base hydrolysis, followed by High Performance Liquid Chromatography purification. All yeast/bacterial cells, media, salts, and buffers were purchased from Fisher Scientific, Sigma-Aldrich, or VWR.

Protein Purification. SLO was expressed in and isolated from $E.\ coli$ BL21(DE3) CodonPlus RIL cultures, as described previously [14,20]. Pure SLO fractions from a final cation exchange column were pooled, exchanged in 0.1 M borate, pH 9.0 buffer. The SLO mutants, L546A and I552A, were constructed previously and prepared in accordance with the wild-type (WT) protein.

Human 15-LOX-2 was expressed in and purified from E. coli Rosetta 2 cells, according to a published protocol [21]. Briefly, overnight starter culture was used to inoculate 2xYT media and grown at 37 °C until OD_{600} reached ~1.0, at which point the incubator temperature was reduced to 18 °C (no IPTG was added). The cultures were harvested 20 h after the temperature decrease. The cell pellet was resuspended in lysis buffer (50 mM NaPO₄, 100 mM NaCl, pH 7.9, 8% glycerol, and 2 mM magnesium sulfate supplemented with lysozyme, DNAse I, and 4-(2-aminoethyl)benzenesulfonyl fluoride) and lysed by sonication. Cell waste was removed by centrifugation and human 15-LOX-2 was isolated from the lysate by passage over a Ni-NTA column. The protein was purified using an imidazole gradient with buffer A (20 mM Tris-HCl, 20 mM imidazole, 500 mM NaCl, pH 8.0) to buffer B (20 mM Tris-HCl, 200 mM imidazole, 500 mM NaCl, pH 8.0). Following initial purification by a Ni-NTA gravity column, human 15-LOX-2 was further purified with by size-exclusion chromatography (SEC) using a HiPrep 26/60 Sephacryl S-200 column on an AKTA FPLC, equilibrated with 50 mM HEPES (pH 7.5), 150 mM NaCl. The running buffer was 50 mM HEPES, 150 mM

*Mo*LOX was expressed in and purified from *P. pastoris* X-33 cells, as described previously [22]. After initial capture of the culture media by hydrophobic interaction chromatography, the protein was eluted by 25 mM potassium phosphate (pH 7) buffer, concentrated and further

purified by SEC using the HiPrep 26/60 Sephacryl S-200 column that was equilibrated in 50 mM HEPES (pH 7.5), 150 mM NaCl. The EndoH-treated form of MoLOX was prepared as described previously [23], and re-isolated by Ni-NTA (to remove EndoH) followed by SEC purification.

Enzyme Kinetics. Steady-state kinetics were performed using a Shimadzu UV-Vis spectrophotometer for SLO and human 15-LOX-2. For MoLOX, the predominant product is a non-conjugated, bis-allylic hydroperoxide formed at the carbon 11 on LA, which can undergo β-fragmentation to generate conjugated hydroperoxide products. Thus, a Hansatech oxygen (O2) electrode was used to measure substrate oxygen consumption in MoLOX reactions. Both instruments were equipped with temperature-controlled water baths. For SLO and MoLOX reactions, the substrate, LA, concentration was varied from 5 to 100 µM and at least six substrate concentrations were measured for constructing a Michaelis-Menten curve. For 15-LOX-2, the substrate concentrations ranged from 1 to 25 μ M; notable substrate inhibition was observed at AA concentrations above 50 µM. Stock substrate concentrations were determined enzymatically based on the product formed from reactions with SLO and product absorbance at 234 nm ($\varepsilon = 23.6 \text{ mM}^{-1} \text{ cm}^{-1}$). The buffers used were 50 mM HEPES, 150 mM NaCl, pH 7.5 for 15-LOX-2 or 50 mM CHES, pH 9.0 for SLO and MoLOX. The addition of sodium chloride for human 15-LOX-2 was necessary to maintain protein stability. We noted an inhibitory effect when TRIS buffers were used with human 15-LOX-2. The temperatures studied were 10, 15, 20, 30, 35, and 40 °C.

For viscosity experiments, buffers were prepared with varying concentrations of trehalose [0, 15, or 30% (w/w)] or glucose [0, 14, 21.5, 26, and 30% (w/w)]. The glucose concentrations correspond to relative viscosities (η/η_0) of 1, 1.5, 2, 2.5, and 3, respectively, when the temperature was set at 20 °C. Note that η_o represents the viscosity of buffer without trehalose or glucose supplemented. For the kinetic measurements of SLO with D2O buffer, CHES was dissolved into 99.5% D2O (Cambridge Isotope labs; Tewksbury, MA 01876) and titrated with dilute NaOD/DCl solutions (in D_2O) to reach a pD of 9.0 (pD = pH_{read} + 0.4). A small volume (2 μL) of SLO stock prepared in H_2O buffer was added to a cuvette in the UV-vis spectrophotometer filled with 980 µL D₂O buffer and substrate (hLA or dLA) prepared in the same D₂O buffer. Upon mixing, the kinetics were immediately initiated and stopped after 1-2 min of data acquisition. During this reaction time, minimal D2O exchange of the protein backbone is expected based on analysis of previous hydrogen deuterium exchange mass spectrometry (HDX-MS) studies [14]. Kinetic parameters were calculated using Igor Pro (v5) software. All kinetic experiments were performed in triplicate.

Differential Scanning Calorimetry (DSC). A TA-instruments Nano-DSC microcalorimeter was used to determine the thermodynamics and stability of the protein samples used. The buffers used were 25 mM HEPES, 150 mM NaCl, pH 7.5 for 15-LOX-2 and 50 mM CHES, pH 9.0 for SLO and MoLOX. For comparison, the thermodynamics of SLO folding were also determined using 50 mM borate, pH 9.0 buffer, at which previous kinetic parameters have been reported [15,24]. When appropriate, the buffers were supplemented with 30% trehalose. Each protein sample was diluted to ${\sim}30~\mu\text{M}$ using their respective buffers. The system was pressurized up to 3 atm. The run was conducted in 'heat' only mode over a temperature range of 30°C–90 °C at a rate of 1 °C/min. The raw data was analyzed using TA-instruments NanoAnalyze software. The data converted to the molar heat capacity. The baseline is integrated using a 4th order polynomial to determine the melting temperature (T_m) and enthalpy of unfolding (ΔH°). After integrating the baseline, the data was fit to two Gaussian models. Experiments were run in duplicate.

3. Results

Viscosity effects on SLO reaction activation energy. Steady-state kinetics were initially measured for the paradigmatic LOX enzyme, SLO. The reaction of SLO with natural substrate, linoleic acid (h-LA), was

performed at pH 9.0, where the kinetic parameters are pH independent, and the C–H cleavage step is rate-determining for $k_{\rm cat}$. Steady-state kinetics for the SLO reaction were obtained in the presence of LA concentrations, ranging from 5 to 100 μ M for both the protium and deuterium substrate and as a function of temperature from 10 to 40 °C. The Arrhenius plot for the reactions with h-LA and d₃₁-LA (deuterated substrate) is shown in Fig. 1. The SLO reaction exhibits a large $^{\rm D}k_{\rm cat}=k_{\rm cat}({\rm H})/k_{\rm cat}({\rm D})$ of ~60 near room temperature, with a weak temperature dependence ($\Delta E_{\rm a}=E_{\rm a}({\rm D})-E_{\rm a}({\rm H})=0.6\pm0.5$ kcal/mol), in agreement with previously published results [14,24].

To test the impact of solvent viscosity on rates, kinetic data were collected in buffers supplemented with trehalose. Trehalose is a naturally occurring, non-reducing disaccharide, consisting of two glucose molecules linked by a 1,1 α , α -glycosidic bond. Trehalose was chosen for the current study as it is known to order water around itself, consequently disrupting the structure and dynamics of bulk water [25,26]. Disaccharides, such as trehalose, generally have a more pronounced impact on the dynamics of bulk water compared to monosaccharides [26]. As such, trehalose has been widely used to study the impact of water on protein structure, stability, and dynamics [27–29]. For the current kinetic study, the viscogen concentration was held constant across the seven temperatures investigated. Note that the viscosity of solvent is sensitive to temperature. For example, a 0.8 M trehalose solution (27% w/w) exhibits a viscosity of $\eta = 2.6$ cP at 20 °C, but decreases to \sim 1.5 cP at 40 °C [30].

SLO steady-state kinetics were recorded in various concentrations of trehalose (0, 15, and 30%). The resulting activation energies (E_a), determined from k_{cat} for h-LA substrate, were virtually unaffected by viscogen (Fig. 1, Table 1). Further, the E_a values for the deuterated substrate (d₃₁-LA) were likewise invariant with trehalose addition (ca. 2.8 kcal/mol). There was no significant impact on the first-order rate constants. However, the second-order rate constant (k_{cat}/K_{m}) at 20 °C for the reaction with h-LA showed a notable decrease from $14\pm3~\mu\text{M}^{-1}$ s^{-1} in osmolyte-free buffer to $9.2 \pm 1 \, \mu M^{-1} \, s^{-1}$, with the addition of 30% trehalose (Table 1). This effect on the second order rate constant was also noted previously, with the magnitude of k_{cat}/K_m decreasing linearly as the relative solution viscosity increases using variable glucose concentrations (Fig. S1A) [31]. The slope of the resulting line for the relationship between the relative $k_{\text{cat}}/K_{\text{m}}$ values as a function of relative solvent viscosity (i.e., $\eta/\eta_0)$ informs on the degree to which diffusion contributes to the rate-limiting step of catalysis. In this graph, a slope of 1 (m = 1) would indicate that substrate binding is rate-limiting, while a slope of 0 (m = 0) would indicate that substrate binding does not contribute significantly to the rate-limiting step of catalysis. The slope for the SLO reaction is ~0.45 (Fig. S1A), consistent with the conclusion [31] that the reaction is partially limited by substrate acquisition.

Effect of solvent viscosity on select SLO active site variants. We next examined the effect of trehalose on the kinetic properties of two SLO mutations at the active site residues, L546 and I552. These residues are

Table 1
Kinetic parameters of SLO variants in the presence and absence of trehalose.^a.

-		_		
SLO variant	[Trehalose] (%)	$k_{\rm cat} ({\rm s}^{-1})^{\rm b}$	$k_{\rm cat}/K_{\rm m}~(\mu{ m M}^{-1}~{ m s}^{-1})^{ m b}$	E _a (kcal/ mol)
WT, h-LA	0	218 ± 15	14 ± 3	2.2 ± 0.6
	30	227 ± 13	9.2 ± 1	2.3 ± 0.4
WT, d-LA	0	3.8 ± 0.3	0.34 ± 0.05	2.8 ± 0.3
	30	4.2 ± 0.4	0.20 ± 0.03	2.7 ± 0.4
L546A	0	1.08 \pm	0.16 ± 0.02	4.1 ± 0.4
		0.03		
	30	$1.27~\pm$	0.10 ± 0.02	3.6 ± 0.3
		0.09		
I552A	0	64 ± 12	2.6 ± 1.2	-0.6 ± 0.2
	30	52 ± 8	$\textbf{2.8} \pm \textbf{1.3}$	-0.2 ± 0.4

^a Buffer: 0.1 M CHES, pH 9.0. When present, trehalose concentration was

^b Temperature, 20 °C.

located along the identified, catalytically-relevant thermal network in SLO (Fig. 2A) [15] and are important for catalysis. For example, the alanine mutation of the conserved Leu clamp (L546), which aids in the positioning of carbon 11 of LA next to the ferric hydroxide cofactor for efficient C–H cleavage, is associated with a 100-fold decrease in $k_{\rm cat}$ and an increased $E_{\rm a}$ from 2 kcal/mol to 4 kcal/mol [24]. I552 sits in the active site, adjacent to L546, but is not predicted to contact substrate directly. The mutation of I552 to volume-reducing Ala, resulted in a 4-fold decrease in $k_{\rm cat}$ and a reduced $E_{\rm a}$ value, from 2 kcal/mol to ca. 0 kcal/mol [15]. Further, the room-temperature X-ray structure of I552A revealed altered sidechain conformations of V750 and a change in conformer populations of L546, implicating that these sidechain conformers are sterically coupled [15].

In the current study, steady-state kinetics were collected for L546A and I552A SLO variants in the absence and presence of 30% trehalose. From the data reported in Fig. 2B and Table 1, there was no effect of increased viscosity on the E_a for either of these catalytically impacted SLO variants. For L546A, the E_a values were 4.1 \pm 0.4 kcal/mol and 3.6 \pm 0.3 kcal/mol for reactions supplemented with 0 and 30% trehalose, respectively. The k_{cat}/K_m for L546A decreased with addition of trehalose, similar to that observed for WT SLO. In contrast, the second-order rate constant for the reaction of I552A was unaffected by increased solvent viscosity (Table 1). The latter is consistent with the trends in the primary deuterium kinetic isotope effects on the second-order rate constants, in which I552A shows no temperature dependence, while WT does [32]. This kinetic feature was rationalized by increased off rates for substrate dissociation from the enzyme through regulation of regional protein dynamics within a defined network that mediates productive substrate binding in SLO [32].

Selection of divergent LOX orthologues. Unlike other fatty acid dioxygenases, such as α -dioxygenase and cyclooxygenases, LOXs are well represented throughout all kingdoms, albeit with low sequence identity and varying kinetic activation barriers among LOX orthologs [33–35]. This offers an ability to examine how divergent enzymes across a family have evolved structurally. With SLO serving as the paradigmatic plant enzyme (Fig. 3A), we selected a representative from each of the animal and fungal kingdoms – human epithelial 15-LOX-2 and M. oryzae LOX.

The human epithelial 15-lipoxygenase-2 (15-LOX-2) was selected as a representative of the animal LOXs, since it is the most well characterized system with kinetic isotope effects reported for its natural substrate, arachidonic acid (AA) [36]. 15-LOX-2 has been structurally solved (Fig. 3B) [21]. The structure includes an N-terminal PLAT (polycystin-1-lipoxygenase α -toxin) domain, which are found in LOXs from higher eukaryotes. The PLAT domain is considered to mediate the interactions with the phospholipid membrane in a Ca^2+-dependent manner, though SLO does not show strong association to membranes [37]. While SLO is also classified as a 15-LOX, these two enzymes only share 28% identity. Notably, 15-LOX-2 (and other animal LOXs) are approximately 150 amino acids shorter than plant LOXs [35], primarily due to the differences in loop structures.

Lipoxygenases from pathogenic fungi exhibit divergent structural features from canonical plant and animal LOXs. For example, they harbor a mononuclear manganese metallocofactor, rather than iron and are decorated with N-linked glycans on the surface [38]. One such fungal LOX originates from the devastating plant pathogen, rice blast fungus *M. oryzae*, that accounts for the loss of \sim 30% of the world's rice crop and is listed as one of the top-10 worst fungal pathogens [39]. Its corresponding lipoxygenase, MoLOX, has been cloned and can be isolated from yeast cultures [40]. The crystal structure of MoLOX has been solved (Fig. 3C) [41]. The fungal LOX lacks the N-terminal PLAT domain found in plant and animal LOXs. Previous kinetic analysis demonstrated that C-H cleavage of LA occurs by hydrogen tunneling and is rate-limiting for both $k_{\rm cat}$ and $k_{\rm cat}/K_{\rm m}$ across the pH range of 7–10 and temperatures 10–30 $^{\circ}\text{C}$ [22]. The temperature range is somewhat limited by the use of an oxygen electrode for monitoring kinetic properties, as the principal reaction product from the oxidation of LA is an unusual bis-allylic hydroperoxide (i.e., 11S-HpODE) [40].

The activation energies, E_a s, for the 15-LOX-2 and MoLOX reactions have been previously characterized, with reported values of ca. 7.2 kcal/mol [36] and 9 kcal/mol [22], respectively. These values are considerably larger than the SLO reaction barrier of 2 kcal/mol (Fig. 3D). Thus, these enzymes provide an opportunity to test the differential effect of viscosity on enzyme family displaying variable activation barriers for hydrogen tunneling.

Effects of solvent viscosity on the MoLOX reaction. Steady-state kinetic measurements were performed for the MoLOX reaction with a range of LA concentrations, from 5 to 100 μM at pH 9. In the presence of 15% or 30% trehalose, the E_a values for the MoLOX were maintained at 8–9 kcal/mol, and thus invariant with increasing solvent viscosity (Fig. 3E, gray trace). Both the k_{cat} and k_{cat}/K_m values were likewise unaffected by addition of trehalose. The latter effect is consistent with our previous viscosity study collected at 20 °C, in which k_{cat} and k_{cat}/K_m exhibited no significant change, even when $\eta=3$ (Fig. S1B). Because of the slow reaction rates and the large uncertainties in the ΔE_a for the MoLOX reaction determined by the oxygen electrode, viscosity effects for the reaction with d-LA were not pursued.

The WT *Mo*LOX enzyme, as isolated from the native fungus or recombinant expressions in yeast cultures, contains a predicted 7–8 sites of *N*-linked glycosylation. These surface post-translational modifications (PTMs) might influence the effect of solvent viscosity on enzyme activity. Thus, we truncated the glycans using endoglycosidase H (endo H), which cleaves the outer sugar structure, leaving a single GlcNac attached to the asparagine sidechain on the protein surface. In the absence of trehalose, the E_a of the EndoH-treated *Mo*LOX is 8.5 ± 1 kcal/mol [23]. Upon addition of 30% trehalose, the corresponding activation energy was determined to be 8.0 ± 0.3 kcal/mol for EndoH-*Mo*LOX. Thus, the activation energies of the *Mo*LOX reaction are not sensitive to the solvent viscosity.

Effects of solvent viscosity on the human 15-LOX-2 reaction. We first examined the pH dependence for the 15-LOX-2 reaction with AA. The

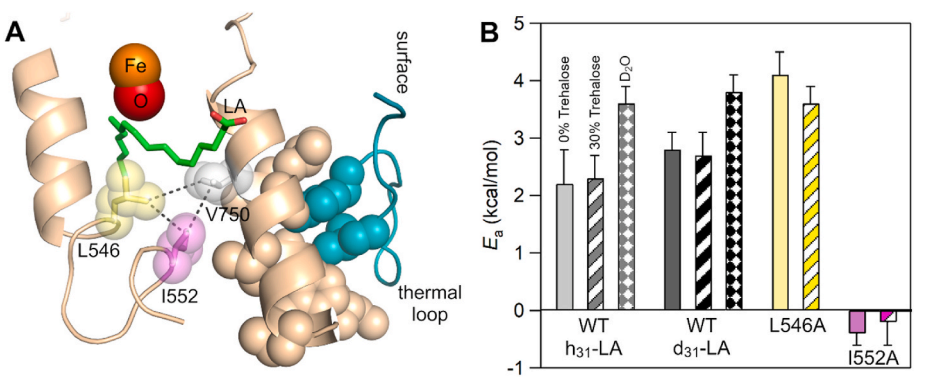


Fig. 2. *A*) Model of the SLO active site. Amino acid sidechains in the putative thermal network, as revealed by room-temperature X-ray [15], stem from the active site to the solvated thermal loop (teal) and are represented as spheres. *B*) Activation energies for the reactions of WT, L546A, and I552A SLO with LA in the absence (solid) and presence (stripes) of 30% trehalose. L546A and I552A reactions were performed with h₃₁-LA substrate only. The WT SLO reaction was also measured in D₂O buffers (no trehalose supplemented), as indicated by the diamond pattern (see Methods for details).

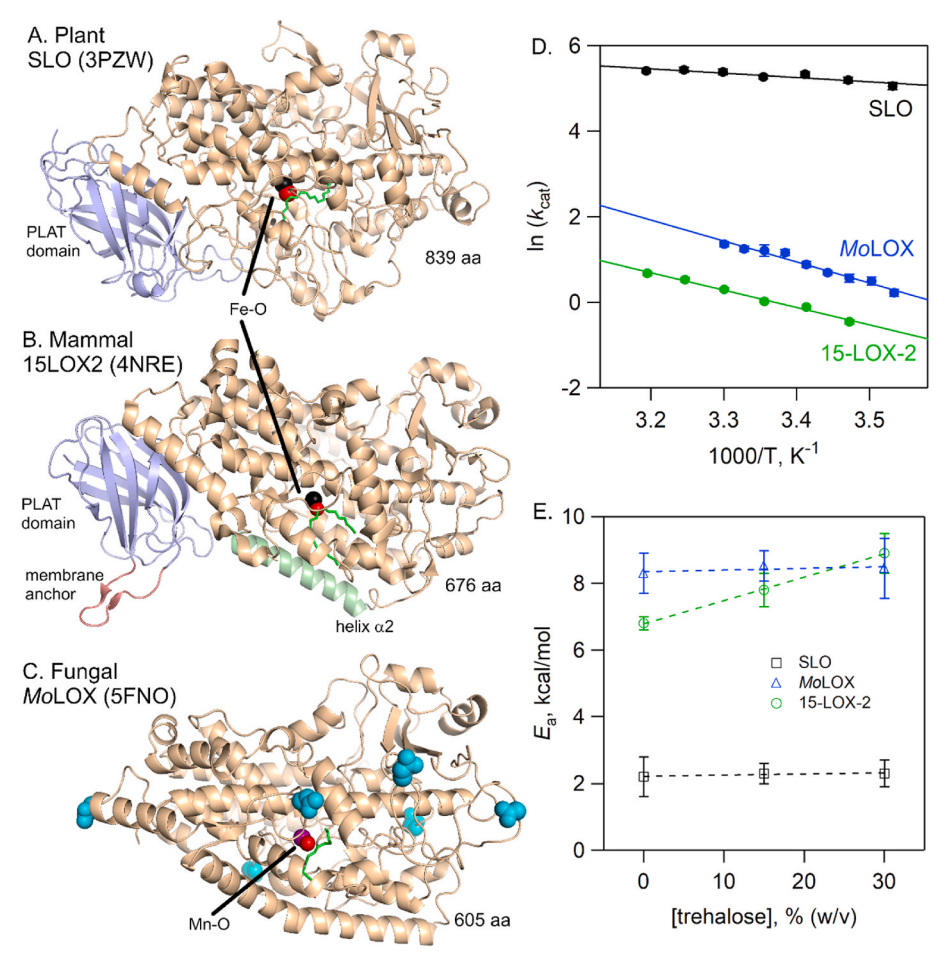


Fig. 3. Structures of representative LOXs, SLO, plant (A); human 15-LOX-2, mammal (B); and MoLOX, fungal (C). The respective PDB id numbers are listed in parentheses. The substrates in (A) and (C) are modeled from previous MD simulations [23]. The N-terminal, PLAT domain is colored light blue in A and B. The cyan spheres represent Asn sidechains that are predicted to be attached to N-linked glycosylation. Panel (D) shows the Arrhenius plots for the reactions of the LOX isozymes. In (E), the activation energies of the LOX reactions are plotted as a function of osmolyte concentration.

first-order rate constants show a virtually pH-independent behavior for the reaction at pH 7.5–9 (Fig. S2). We focused our kinetic study on pH 7.5, where select kinetic studies previously reported KIEs [36]. The 15-LOX-2 reaction kinetics were measured across six AA concentrations, from 1 to 25 μ M; at AA concentrations of 50 μ M or above, substrate inhibition was observed. In the absence of trehalose, the activation energy for the 15-LOX-2 reaction at pH 7.5 is 6.8 \pm 0.2 kcal/mol, which is in good agreement with a value of \sim 7.2 kcal/mol, estimated from previously reported set of $k_{\rm cat}$ values collected across a narrower range of temperatures [36]. When trehalose was supplemented in the reaction, the $E_{\rm a}$ increased significantly from 6.8 kcal/mol to 7.8 kcal/mol for 15% and to 8.9 kcal/mol for 30% trehalose (Fig. 3E). The increased $E_{\rm a}$ values were also accompanied by decreased $k_{\rm cat}$ values.

We also examined the effect of the nature of the viscogen and its effect on substrate binding. In buffers containing glucose, the 15-LOX-2 reaction rates with AA were also inhibited (Fig. 4). As the relative viscosity (η/η_0) was increased from unity (0% w/w glucose) to 3(30% w/w)glucose), the first-order rate constant decreased in a glucose concentration dependent manner (Fig. 4A). To quantify this effect, we plotted the relative first-order rate constants, $(k_{cat})_0/(k_{cat})_n$, versus relative viscosity (Fig. 4B, empty triangles). The terms, $(k_{cat})_0$ and $(k_{cat})_{\eta}$, represent the first-order rate constants for the 15-LOX-2 reaction without and with glucose supplemented in the buffer, respectively. With an observed slope of 0.7 (m = 0.7) for the viscosity effect on the first order rate constant, the plot in Fig. 4B supports that the 15-LOX-2 reaction rate is inhibited by glucose. For comparison, the relative second-order rate constant, $(k_{cat}/K_m)_0/(k_{cat}/K_m)_\eta$, on the same plot (Fig. 4B, solid dots), was nearly independent of viscosity (m \sim 0). These data indicate that the 15-LOX-2 reaction is not significantly diffusional controlled.

To further explore the inhibitory behavior of solvent viscosity on

animal LOXs, we collected kinetics for the coral 8R-LOX reaction with AA, in both the absence and presence of 30% glucose (Fig. S3). A comparable trend was observed for this reaction, with an apparent drop in the activity within the substrate concentration range used for this study. The elevated apparent K_m values precluded a more comprehensive kinetic study. The inhibitory effect from viscogens on human lipoxygenase activity was also noted previously for 15-LOX-1 and 12-LOX [42]. The cumulative data suggest that animal LOXs share a general inhibitory feature in solutions with elevated viscosity.

Viscosity effects on protein folding stability. Trehalose is also known to enhance protein stability; as such, it is often used as a cryo-protectant [28]. To demonstrate the impact of trehalose solutions on the protein folding stability, we carried out differential scanning calorimetry (DSC) experiments on these LOXs in buffers absent and supplemented with 30% trehalose. The DSC thermogram revealed a single peak for the three LOX orthologues (Fig. S4), consistent with their monomeric species. Analysis of the DSC thermograms collected for SLO in 0.1 M CHES buffer show an enthalpy (ΔH°) of 347 \pm 14 kcal/mol and melting temperature (T_m) of 65.6 \pm 0.4 °C (Table 2). Supplementation of 30% trehalose to the buffer did not influence the ΔH° , though the T_m increased by ca. 4 °C. Extension of DSC experiments to assess trehalose effects on the structural stabilities of MoLOX and 15-LOX-2 reveal similar trends to SLO, with increases in the $T_m s$ by 4–5 $^{\circ} C$ with addition of 30% trehalose (Table 2). Note that the varying magnitudes of the folding enthalpies are consistent with the sizes of the proteins. MoLOX and 15-LOX-2 are considerably smaller than SLO (839 aa), with 605 and 676 (696 including the N-terminal His tag) amino acids, respectively. Importantly, the lack of viscosity effect on the enthalpy of protein stability for 15-LOX-2 rules out protein instability as the source of the observed inhibition on the first-order rate constants.

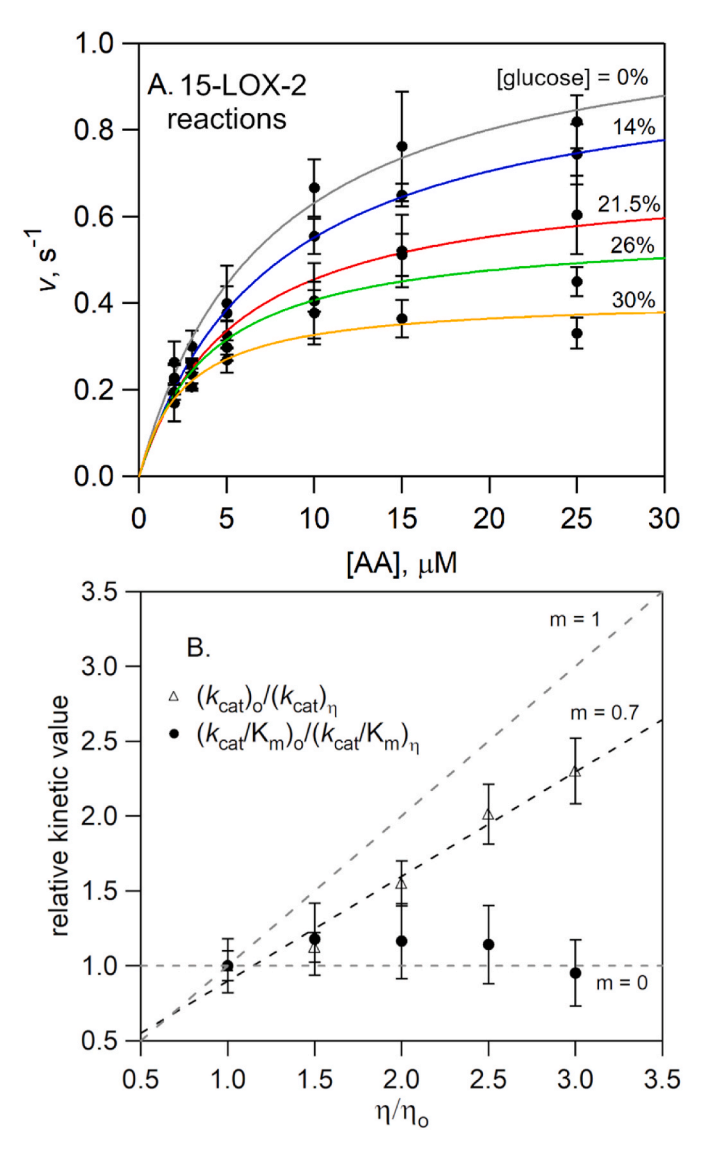


Fig. 4. Effects of glucose supplementation on the kinetic properties for the reaction of 15-LOX-2 with AA. (A) Michaelis-Menten plots for the 15-LOX-2 reaction with AA in various concentrations of glucose (shown in w/w percentages). The temperature was maintained at 20 $^{\circ}\text{C}$ and the buffer included 50 mM HEPES, 150 mM NaCl, pH 7.5. (B) Plot of relative rate constants (defined in the figure legend) versus relative viscosity, η/η_{o} , where η_{o} represents the buffer with no glucose added.

 Table 2

 DSC thermodynamic parameters for LOX protein folding.

LOX variant	ΔH ^o (kcal/mol)		T _m (°C)		ΔT_m (°C)
	0%ª	30% ^a	0%ª	30%ª	
SLO MoLOX 15LOX2	347 ± 14 133 ± 26 191 ± 10	346 ± 8 140 ± 14 178 ± 3	65.6 ± 0.4 55.1 ± 0.4 52.8 ± 0.3	70.0 ± 0.1 60.2 ± 0.2 56.7 ± 0.1	4.4 ± 0.5 5.1 ± 0.4 3.9 ± 0.3

^a Concentration of trehalose supplemented in the buffers.

4. Discussion

Solvent-slaved Motions Linked to Hydrogen Tunneling in SLO. In the current study, we present a kinetic characterization of the solvent viscosity effects on the activation barrier for hydrogen tunneling in the oxidation of fatty acids by representatives across the LOX family. For the plant representative, SLO, there was no change in the reaction rates or

activation energy associated with the transfer of hydrogen or deuteron atoms, across a range of trehalose concentrations. There is an emerging view that favors the 'preferential hydrational' model [29], in which trehalose influences protein stability through disruption of the structure and dynamics of bulk water properties, with little-to-no impact of the 'biological' water layer interacting with the surface of the protein. This model is supported by the DSC-detected increase in the T_m of SLO, with no significant change in the folding ΔH^{o} , when the buffer was supplemented with 30% trehalose.

Temperature dependent HDX-MS was previously applied to a series of SLO variants, including WT, L546A, and I553G (and later I552A [15]), each displaying varying E_a values of catalysis. The investigation detected correlated activation energies for H/D exchange – a metric for local peptide flexibility – and catalysis at a remote, solvent exposed surface loop consisting of residues 317–334 (Fig. 2A, teal) [14]. From analysis of the SLO structure, a catalytically linked, anisotropic thermal conduit was proposed that stretches from this surface loop to the active site, through several aliphatic sidechains exhibiting multiple conformers (Fig. 2A), including the functionally important active site residues. Note that in the current study, we observed no solvent viscogen effects on $k_{\rm cat}$ or E_a for either L546A or I552A (Fig. 2B).

Subsequent temperature dependent, nanosecond-resolved fluorescent Stokes shifts, using a fluorophore (as a probe for kinetic detection) appended to SLO at position 322 in the middle of this identified thermal loop [43], measured identical activation energies between the solvent relaxation surrounding the photo-induced dipole moment and the catalytic E_a [15]. Importantly, the work implicated solvent dynamics to mediate a long-range, cooperative, and anisotropic reorganization of the protein as the source of the activation barrier for hydrogen tunneling in SLO. Taken together with the results from the current kinetic investigation, we conclude that the protein thermal motions that comprise the enthalpy activation barrier for hydrogen tunneling in SLO are slaved to the hydration shell adjacent to the identified surface loop.

Of note, we did observe an increase in the activation energy for the SLO reaction when deuterium oxide buffers were employed (Fig. 2B, diamonds). Deuterium oxide can influence both the solvent viscosity and local protein hydrophobicity, as well as the flexibility and stability of proteins [44,45], and therefore its effect on enzyme activity can be complicated. However, given the relatively short timescale of the kinetic experiment (≤ 1 min), moderate-to-little backbone exchange is expected during the brief exposure of the protein to heavy water, based on previous HDX-MS analysis [14,46].

Viscosity-Sensitive Conformational Changes in Animal LOXs. In contrast to SLO, the $k_{\rm cat}$ for the 15-LOX-2 reaction decreased with increasing solvent viscosity (Fig. 4). Viscosity-sensitive rate constants can reflect conformational motions associated with catalysis and/or product release [47]. Given the magnitude of the primary deuterium kinetic isotope effect (>30) for the 15-LOX-2 reaction with AA [36], the C–H bond cleavage step by tunneling is rate-limiting for $k_{\rm cat}$. Thus, the kinetic data reported here suggest that viscosity-dependent conformational motions in 15-LOX-2 are linked to the chemical step. These conformational motions will be different than the nature of the more subtle, protein thermal fluctuations that mediate thermal energy transfer from the surface-exposed thermal loop in SLO.

One possibility for the conformational change(s) in 15-LOX-2 may involve helix $\alpha 2$ (H $\alpha 2$). This helix lines the substrate portal in all LOXs. In select animal LOXs (e.g., human 5-LOX and coral 11*R*-LOX), the H $\alpha 2$ adopts a 'closed' conformation, which requires a conformational change to permit access for substrate binding [48,49]. Based on the X-ray structure of 15-LOX-2, H $\alpha 2$ is in an 'open' conformation (Fig. 3B) [21]. This structure was solved with a substrate mimic, C8E4, in the active site channel; there are no current structures available of a substrate-free form. Previous HDX-MS analysis of 15-LOX-2 in the presence of a selective inhibitor showed rigidification of H $\alpha 2$ [46]. Another HDX-MS study with substrate AA likewise showed altered dynamics for a short segment of H $\alpha 2$ [50]. These cumulative HDX results indicate that the

structure and dynamics of this helical segment in 15-LOX-2 are sensitive to the occupancy of the active site.

Human and other animal LOXs are also allosterically regulated. For example, the binding of the anti-inflammatory molecule, 3-acetyl-11-keto-beta-boswellic acid, to human 5-LOX shifts the enzyme's product distribution from 5-HETE to 12-HETE [51]. The change in regiospecificity may be influenced by the structure and/or dynamics of H α 2. Select animal LOXs can even dimerize along H α 2, with a change in oligomerization influencing enzyme rates [52–54]. Further, allosteric changes in human 15-LOX-2 reactivity have also been reported [55,56]. While dynamic allosteric effects have also been detected in the plant enzyme of SLO [20,57], the effects on catalysis are subtle compared to the animal LOXs.

Note that the inhibitory effect on $k_{\rm cat}$ reported here for 15-LOX-2 varies slightly from the observations by Wecksler et al., in which they reported a nearly invariant $k_{\rm cat}$ value between 0 and 30% glucose [36]. While the temperatures studied were different (37 °C vs 20 °C here), the difference in trends of $k_{\rm cat}$ is likely attributed to the supplementation of sodium chloride to the reaction buffers in the current study. As determined by DSC, the protein folding thermodynamics were found to be sensitive to the addition of NaCl, in which the enthalpy of folding was increased from ca. 140 kcal/mol to 190 kcal/mol from adding 0–150 mM NaCl. Supplementing the buffers with 0.15 M NaCl was found to enhance the stability of the 15-LOX-2 protein.

Comparisons to Enzymatic Hydride Tunneling. There are several examples of solvent studies on enzymes catalyzing the quantum mechanical transfer of hydride ion (H⁻), with variable dependence on solution viscosity. For example, viscogen sensitive rate constants were observed for the human orthologue of glycoxylate oxidase and Pseudomonas Lphenylalanine oxidase [19,58]. In dihydrofolate reductase, the reaction rates were sensitive to the addition of co-solvents, but the main inhibitory effect was attributed to solvent dielectric rather than viscosity [59]. Other enzyme systems presented viscogen independent rate constants and/or KIEs for hydride tunneling [60-62]. Of note, a comparative study of solvent effects was performed on a family of protochlorophyllide oxidoreductase (POR) enzymes from bacteria and plants [62]. From this investigation, cyanobacterial PORs displayed significant changes in the activation energies for the proton transfer step while the hydride tunneling steps were both unaffected by viscosity and nearly invariant across the family. The work suggested an evolutionary relationship between hydride tunneling efficiency in enzymes and the tuning of protein dynamics, as also supported from laboratory evolved enzymes [63].

One possible explanation for the differing kinetic properties emerging from these solvent viscosity studies on enzymatic hydride transfer may be related to the magnitude of the temperature dependence of the KIE [61]. In select hydride tunneling systems, such as reported in Refs. [60–62], strong temperature dependences were observed (i.e., ΔE_a > 1 kcal/mol) that have been suggested to arise from promoting motion (s) coupled to the chemical step [2,61]. In these cases, the protein motions are not sensitive to the presence of viscogens. Whereas in SLO, hydrogen (neutral) transfer is also not sensitive to the solution viscosity and yet this enzyme system has a weakly temperature dependent KIE. Similarly, in a bacterial methylamine dehydrogenase that displays ΔE_a \approx 0 kcal/mol for a hydrogen tunneling process, the kinetic properties, including isotope effects, were not affected by the addition of 30% glycerol [64]. It is important to note that there is a fundamental distinction between the transfer of hydride (H⁻) versus a neutral hydrogen atom (H•). The transfer of charge, as in the case of hydride tunneling, has strong electronic coupling and behave more adiabatic relative to neutral H atom transfer [65]. As a consequence, enzyme-catalyzed hydride transfer reactions are often associated with the observation of semiclassical or 'normal' primary deuterium kinetic isotope effects (≤7). Conversely, hydrogen atom tunneling in enzyme C-H activation reactions, as in LOXs, exhibit primary deuterium KIEs (20-100) well in excess of the classical limit and accompanied by weak to no temperature dependence [12].

In summary, the current study represents an in-depth kinetic study of the role of solvent viscosity on the catalytic properties of representative LOXs, in which the rate-limiting, formal hydrogen transfer reaction occurs by a deep tunneling mechanism. The rate constants and activation barrier for hydrogen tunneling in the model plant LOX, SLO, were unaffected by increasing the solvent viscosity. The lack of viscosity effects in the case of SLO is significant and underpins that hydrogen tunneling is not mediated by viscogen sensitive, large-scale conformational rearrangements. Thus, our study posits that the enthalpically driven protein thermal motions that comprise the activation energy barrier for hydrogen tunneling are slaved to the water dynamics at the protein's hydration shell. In contrast to our findings for SLO, human 15-LOX-2 and coral 8R-LOX were inhibited by viscogens, indicating that viscogen sensitive, conformational changes accompany catalysis in animal LOXs. Our results show that enzymes catalyzing the same reaction across different kingdoms can have either viscosity dependent or independent protein conformational motions. Collectively, these kinetic features provide insight into the roles of the solvent layers in facilitating hydrogen tunneling across plant and animal LOX reactions.

Acknowledgements

The work was supported by the National Science Foundation (CLP 20-03956 and MCB 22-31079 to ARO). Melissa Gouge was supported by NSF summer REU (18-51844).

Appendix A. Supplementary data

Supplementary data to this article can be found online at https://doi.org/10.1016/j.abb.2023.109740.

References

- S. Hammes-Schiffer, Hydrogen tunneling and protein motion in enzyme reactions, Acc. Chem. Res. 39 (2006) 93–100.
- [2] S. Hay, N.S. Scrutton, Good vibrations in enzyme-catalysed reactions, Nat. Chem. 4 (2012) 161–168.
- [3] J.P. Klinman, A. Kohen, Hydrogen tunneling links protein dynamics to enzyme catalysis, Annu. Rev. Biochem. 82 (2013) 471–496.
- [4] A.V. Soudackov, S. Hammes-Schiffer, Proton-coupled electron transfer reactions: analytical rate constants and case study of kinetic isotope effects in lipoxygenase, Faraday Discuss 195 (2016) 171–189.
- [5] J.P. Klinman, A.R. Offenbacher, S. Hu, Origins of enzyme catalysis: experimental findings for C-H activation, new models, and their relevance to prevailing theoretical constructs, J. Am. Chem. Soc. 139 (2017) 18409–18427.
- [6] H. Frauenfelder, G. Chen, J. Berendzen, P.W. Fenimore, H. Jansson, B. H. McMahon, I.R. Stroe, J. Swenson, R.D. Young, A unified model of protein dynamics, Proc. Natl. Acad. Sci. U.S.A. 106 (2009) 5129–5134.
- [7] J.R. Lewandowski, M.E. Halse, M. Blackedge, L. Emsley, Direct observation of hierchical protein dynamics, Science 348 (2015) 578–581.
- [8] M.-C. Bellissent-Funel, A. Hassanali, M. Havenith, R. Henchman, P. Pohl, F. Sterpone, D. van der Spoel, Y. Xu, A.E. Garcia, Water determines the structure and dynamics of proteins, Chem. Rev. 116 (2016) 7673–7697.
- [9] I. Feussner, C. Wasternack, The lipoxygenase pathway, Annu. Rev. Plant Biol. 53 (2002) 275–297.
- [10] J.Z. Haeggstrom, C.D. Funk, Lipoxygenase and leukotriene pathways: biochemistry, biology, and roles in disease, Chem. Rev. 111 (2011) 5866–5898.
- [11] I. Ivanov, D. Heydeck, K. Hofheinz, J. Roffeis, V.B. O'Donnell, H. Kuhn, M. Walther, Molecular enzymology of lipoxygenases, Arch. Biochem. Biophys. 503 (2010) 161–174.
- [12] J.P. Klinman, A.R. Offenbacher, Understanding biological hydrogen transfer through the lens of temperature dependent kinetic isotope effects, Acc. Chem. Res. 51 (2018) 1966–1974.
- [13] J.P. Klinman, Importance of protein dynamics during enzymatic C-H bond cleavage catalysis, Biochemistry 52 (2013) 2068–2077.
- [14] A.R. Offenbacher, S. Hu, E.M. Poss, C.A. Carr, A.D. Scouras, D.M. Prigozhen, A. T. Iavarone, A. Palla, T. Alber, J.S. Fraser, J.P. Klinman, Hydrogen-deuterium exchange of lipoxygenase uncovers a relationship between distal, solvent exposed protein motions and the thermal activation barrier for catalytic proton-coupled electron tunneling, ACS Cent. Sci. 3 (2017) 570–579.
- [15] J.P. Zaragoza, A.R. Offenbacher, S. Hu, C.L. Gee, Z.M. Firestein, N. Minnetian, Z. Deng, F. Fan, A.T. Iavarone, J.P. Klinman, Temporal and spatial resolution of distal protein motions that activate hydrogen tunneling in soybean lipoxygenase, Proc. Natl. Acad. Sci. U.S.A. 120 (2023), e2211630120.

- [16] A. Ansari, C.M. Jones, E.R. Henry, J. Hofrichter, W.A. Eaton, The role of solvent viscosity in the dynamics of protein conformational changes, Science 256 (1992) 1796–1798.
- [17] P.W. Fenimore, H. Frauenfelder, B.H. McMahon, F.G. Parak, Slaving: solvent fluctuations dominate protein dynamics and functions, Proc. Natl. Acad. Sci. U.S.A. 99 (2002) 16047–16051.
- [18] C. Feng, R.V. Kedia, J.T. Hazzard, J.K. Hurley, G. Tollin, J.H. Enemark, Effect of solution viscosity on intramolecular electron transfer in sulfite oxidase, Biochemistry 41 (2002) 5816–5821.
- [19] E. Romero, S.T. Ladani, D. Hamelberg, G. Gadda, Solvent-slaved motions in the hydride tunneling reaction catalyzed by human glycolate oxidase, ACS Catal. 6 (2016) 2113–2120.
- [20] D.E. Roberts, A.M. Benton, C. Fabian-Bayola, A.M. Spuches, A.R. Offenbacher, Thermodynamic and biophysical study of fatty acid effector binding to soybean lipoxygenase: implications for allostery driven by helix α2 dynamics, FEBS Lett. 596 (2022) 350–359.
- [21] M.J. Kobe, D.B. Neau, C.E. Mitchell, S.G. Bartlett, M.E. Newcomer, The structure of human 15-lipoxygenase-2 with a substrate mimic, J. Biol. Chem. 289 (2014) 8562–8569.
- [22] A. Kostenko, K. Ray, A.T. Iavarone, A.R. Offenbacher, Kinetic characterization of the C-H activation step for the lipoxygenase from the pathogenic fungus *Magnaporthe oryzae*: impact of N-linked glycosylation, Biochemistry 58 (2019) 3193–3203.
- [23] A. Sharma, C. Whittington, M. Jabed, G.S. Hill, A. Kostenko, T. Yu, P. Li, P.E. Doan, B.M. Hoffman, A.R. Offenbacher, 13C Electron nuclear double resonance spectroscopy-guided molecular dynamics computations reveal the structure of the enzyme-substrate complex of an active, N-linked glycosylated lipoxygenase, Biochemistry (2023).
- [24] M.J. Knapp, K. Rickert, J.P. Klinman, Temperature-dependent isotope effects in soybean lipoxygenase-1: correlating hydrogen tunneling with protein dynamics, J. Am. Chem. Soc. 124 (2002) 3865–3874.
- [25] S. Magazu, F. Migliardo, M.T.F. Telling, Study of the dynamical properties of water in disaccharide solutions, Eur. Biophys. J. 36 (2007) 163–171.
- [26] M. Heyden, E. Brundermann, U. Heugen, G. Niehues, D.M. Leitner, M. Havenith, Long-range influence of carbohydrates on the solvation dynamics of water answers from terahertz absorption measurements and molecular modeling simulations, J. Am. Chem. Soc. 130 (2008) 5773–5779.
- [27] L. Cordone, G. Cottone, S. Giuffrida, G. Palazzo, G. Venturoli, C. Viappiani, Internal dynamics and protein-matrix coupling in trehalose-coated proteins, Biochim. Biophys. Acta 1749 (2005) 252–281.
- [28] N.K. Jain, I. Roy, Effect of trehalose on protein structure, Protein Sci. 18 (2009) 24–36.
- [29] C. Olsson, H. Jansson, J. Swenson, The role of trehalose for the stabilization of proteins, J. Phys. Chem. B 120 (2016) 4723–4731.
- [30] J.G. Sampedro, R.A. Munoz-Clares, Trehalose-mediated inhibition of the plasma membrane H⁺-ATPase from *Kluyveromyces lactis*: dependence on viscosity and temperature, J. Bacteriol. 184 (2002) 4384–4391.
- [31] M.H. Glickman, J.P. Klinman, Nature of rate-limiting steps in the soybean lipoxygenase-1 reaction, Biochemistry 34 (1995) 14077–14092.
- [32] S. Hu, A.R. Offenbacher, E.D. Lu, J.P. Klinman, Comparative kinetic isotope effects on first- and second-order rate constants of soybean lipoxygease variants uncover a substrate-binding network, J. Biol. Chem. 294 (2019) 18069–18076.
- [33] C. Schneider, D.A. Pratt, N.A. Porter, A.R. Brash, Control of oxygenation in lipoxygenase and cyclooxygenase catalysis, Chem. Biol. 14 (2007) 473–488.
- [34] A. Mosblech, I. Feussner, I. Heilmann, Oxylipins: structurally diverse metabolites from fatty acid oxidation, Plant Phys. Biochem. 47 (2009) 511–517.
- [35] M.E. Newcomer, A.R. Brash, The structural basis for specificity in lipoxygenase catalysis, Protein Sci. 24 (2015) 298–309.
- [36] A.T. Wecksler, V. Kenyon, N.K. Garcia, J.D. Descampes, W.A. van der Donk, T. R. Holman, Kinetic and structural investigations of the allosteric site in human epithelial 15-lipoxygenase-2, Biochemistry 48 (2009) 8721–8730.
- [37] D.L. Rohlik, E. Patel, N.C. Gilbert, A.R. Offenbacher, B.L. Garcia, Investigating membrane-binding properties of lipoxygenases using surface plasmon resonance, Biochem. Biophys. Res. Commun. 670 (2023) 47–54.
- [38] E.H. Oliw, Iron and manganese lipoxygenases of plant pathogenic fungi and their role in biosynthesis of jasmonates, Arch. Biochem. Biophys. 722 (2022), 109169.
- [39] R.A. Wilson, N.J. Talbot, Under pressure: investigating the biology of plant infection by Magnaporthe oryzae, Nat. Rev. Microbiol. 7 (2009) 185–195.
- [40] A. Wennman, F. Jerneren, A. Magnuson, E.H. Oliw, Expression and characterization of manganese lipoxygenase of the rice blast fungus reveals prominent sequential lipoxygenation of α-linolenic acid, Arch. Biochem. Biophys. 583 (2015) 87–95.
- [41] A. Wennman, E.H. Oliw, S. Karkehabadi, Y. Chen, Crystal structure of manganese lipoxygenase of the rice blast fungus *Magnaporthe oryzae*, J. Biol. Chem. 291 (2016) 8130–8139.

- [42] E.N. Seagraves, T.R. Holman, Kinetic investigations of the rate-limiting step in human 12- and 15-lipoxygenase, Biochemistry 42 (2003), 52365243.
- [43] J.P. Zaragoza, A. Nguy, N. Minnetian, Z. Deng, A.T. Iavarone, A.R. Offenbacher, J. P. Klinman, Detecting and characterizing the kinetic activation of thermal networks in proteins: thermal transfer from a distal, solvent-exposed loop to the active site in soybean lipoxygenase, J. Phys. Chem. B 123 (2019) 8662–8674.
- [44] P. Cioni, G.B. Strambini, Effect of heavy water on protein flexibility, Biophys. J. 82 (2002) 3246–3253.
- [45] Y.M. Efimova, S. Haemers, B. Wierczinski, W. Norde, A.A. van Well, Stability of globular proteins in H₂O and D₂O, Biopolymers 85 (2007) 264–273.
- [46] W.-C. Tsai, N.C. Gilbert, A. Ohler, M. Armstrong, S. Perry, C. Kalyanaraman, A. Yasgar, G. Rai, A. Simeonov, A. Jadhav, M. Standley, H.-W. Lee, P. Crews, A. T. Iavarone, M.P. Jacobson, D.B. Neau, A.R. Offenbacher, M.E. Newcomer, T. R. Holman, Kinetic and structural investigations of novel inhibitors of human epithelial 15-lipoxygenase-2, Bioorg, Med. Chem. 46 (2021), 116349.
- [47] G. Gadda, P. Sobrado, Kinetic solvent viscosity effects as probes for studying the mechanisms of enzyme action, Biochemistry 57 (2018) 3445–3453.
- [48] N.C. Gilbert, S.G. Bartlett, M.T. Waight, D.B. Neau, W.E. Boeglin, A.R. Brash, M. E. Newcomer, The structure of human 5-lipoxygenase, Science 331 (2011) 217–219
- [49] P. Eek, R. Jarving, N.C. Gilbert, M.E. Newcomer, N. Samel, Structure of a calcium-dependent 11R-lipoxygenase suggests a mechanism for Ca²⁺ regulation, J. Biol. Chem. 287 (2012) 22377–22386.
- [50] K.D. Droege, M.E. Keithly, C.R. Sanders, R.N. Armstrong, M.K. Thompson, Structural dynamics of 15-lipoxygenase-2 via hydrogen-deuterium exchange, Biochemistry 56 (2017) 5065–5074.
- [51] N.C. Gilbert, J. Gerstmeier, E.E. Schexnaydre, F. Borner, U. Garscha, D.B. Neau, O. Werz, M.E. Newcomer, Structural and mechanistic insights into 5-lipoxygenase inhibition by natural products, Nat. Chem. Biol. 16 (2020) 783–790.
- [52] A.-K. Hafner, M. Cernescu, B. Hofmann, M. Ermisch, M. Hornig, J. Metzner, G. Schneider, B. Brutschy, D. Steinhilber, Dimerization of human 5-lipoxygenase, Biol. Chem. 392 (2011) 1097–1111.
- [53] I. Ivanov, W. Shang, L. Toledo, L. Masgrau, D.I. Svergun, S. Stehling, H. Gomez, A. Di Venere, G. Mei, J.M. Lluch, E. Skrzypczak-Jankun, A. Gonzalez-Lafont, K. Kuhn, Ligand-induced formation of transient dimers of mammalian 12/15-lip-oxygenase: a key to allosteric behavior of this class of enzymes? Proteins 80 (2011) 703–712.
- [54] W.-C. Tsai, A.M. Aleem, C. Whittington, W.A. Cortopassi, C. Kalyanaraman, A. Baroz, A.T. Iavarone, E. Skrzypczak-Jankun, M.P. Jacobson, A.R. Offenbacher, T.R. Holman, Mutagenesis, hydrogen-deuterium exchange, and molecular docking investigations establish the dimeric interface of human platelet-type 12lipoxygenase, Biochemistry 60 (2021) 802–812.
- [55] N. Joshi, E.K. Hoobler, S. Perry, G. Diaz, B. Fox, T.R. Holman, Kinetic and structural investigations into the allosteric and pH effect on substrate specificity of human epithelial 15-lipoxygenase-2, Biochemistry 52 (2013) 8026–8035.
- [56] S.E. Wenzel, Y.Y. Tyurina, J. Zhao, C.M. St. Croix, H.H. Dar, G. Mao, V.A. Tyurin, T. S. Anthonymuthu, A.A. Kapralov, A.A. Amoscato, K. Mikulska-Ruminska, I. H. Shrivastava, E.M. Kenny, Q. Yang, J.C. Rosenbaum, L.J. Sparvero, D.R. Emlet, X. Wen, Y. Minami, F. Qu, S.C. Watkins, T.R. Holman, A.P. VanDemark, J. A. Kellum, I. Bahar, H. Bayir, V.E. Kagan, PEBP1 wardens ferroptosis by enabling lipoxygenase generation of lipid death signals, Cell 171 (2017) 628–641.
- [57] A.R. Offenbacher, T.R. Holman, Fatty acid allosteric regulation of C-H activation in plant and animal lipoxygenases, Molecules 25 (2020) 3374.
- [58] Y. Ohta, E.B. Mukouyama, H. Suzuki, Kinetic isotope effect on the L-phenylalanine oxidase from *Pseudomonas* sp. P-501, J. Biochem. 139 (2006) 551–555.
- [59] E.J. Loveridge, L.-H. Tey, R.K. Allemann, Solvent effects on catalysis by Escherichia coli dihydrofolate reductase, J. Am. Chem. Soc. 132 (2010) 1137–1143.
- [60] D.j. Heyes, M. Sakuma, N.S. Scrutton, Solvent-slaved protein motions accompany proton but not hydride tunneling in light-activated protochlorophyllide oxidoreductase, Angew. Chem. 48 (2009) 3850–3853.
- [61] S. Hay, C.R. Pudney, M.J. Sutcliffe, N.S. Scrutton, Are environmentally coupled enzymatic hydrogen tunneling reactions influenced by changes in solvent viscosity? Angew. Chem. 47 (2008) 537–540.
- [62] D.J. Heyes, C. Levy, M. Sakuma, D.L. Robertson, N.S. Scrutton, A twin-track approach has optimized proton and hydride transfer by dynamically coupled tunneling during hte evolution of protocholorphyllide oxidoreductase, J. Biol. Chem. (2011) 286.
- [63] P. Singh, A. Vandemeulebroucke, J. Li, C. Schulenburg, G. Fortunato, A. Kohen, D. Hilvert, C. Cheatum, Evolution of the chemical step in enzyme catalysis, ACS Catal. 11 (2021) 6726–6732.
- [64] J. Basran, M.J. Sutcliffe, N.S. Scrutton, Enzymatic H-transfer requires vibrationdriven extreme tunneling, Biochemistry 38 (1999) 3218–3222.
- [65] Z.D. Nagel, J.P. Klinman, Tunneling and dynamics in enzymatic hydride transfer, Chem. Rev. 106 (2006) 3095–3118.